Sharp-interface simulations of drop deformation in electric fields

Knut Erik Teigen
Norwegian University of Science and Technology (NTNU)
Department of Energy and Process Engineering
Kolbjørn Hejes v 1B, NO-7491 Trondheim, Norway

and **Svend Tollak Munkejord**
SINTEF Energy Research
Energy Processes
NO-7465 Trondheim, Norway

ABSTRACT

This paper describes numerical simulations of two-phase electrohydrodynamics using a sharp-interface method. Simulations are performed on typical test cases from the literature, and the results are compared to methods that use a smeared interface. The results show that the sharp-interface method gives significant improvements in accuracy.

Index Terms — **Numerical analysis, electrohydraulics, dielectric materials, finite difference methods, hydrodynamics, interface phenomena.**

1 INTRODUCTION

ELECTROHYDRODYNAMIC flows are in general very complex due to the interactions between electric forces and flow dynamics, and analytical results are limited to simplified setups. The addition of more than one phase to the system further complicates the analysis. This inherent complexity encourages the use of numerical methods to gain additional insight into the physical phenomena.

Early numerical simulations of electrohydrodynamics typically assume either Stokes flow or inviscid flow, which makes it possible to formulate the problem using integral equations. These equations can then be efficiently solved using the boundary-element method (BEM). In [1], the deformation of a drop was studied using this approach, and in [2], the interaction between drop pairs was investigated.

In [3] and [4], a finite-element method which allowed a solution at finite Reynolds numbers was employed to study drop deformation in electric fields. It concluded that while the creeping-flow assumption was valid for low drop deformations, it was not able to predict phenomena occurring for higher deformations.

The methods mentioned so far do not take into account topological changes, e.g. the merging and breakup of drops. Recently, numerical methods have been developed that allow such topological changes. In the seminal paper [5], a front-tracking method was presented that uses a set of connected marker points to represent the interface. The handling of topological changes is fairly complex. First, a search has to be made among the front elements to identify situations where a topology change is needed. Then, the elements have to be updated to account for the change. Additionally, when the interface is stretched, restructuring of the interface is necessary to maintain sufficient accuracy. This is a complicated process, especially in three dimensions. The jumps in physical properties across the interface is handled using smoothing. In [6], the front-tracking method was extended to account for electric fields, and the distribution of drops in a channel was investigated. This study, however, did not take the merging of colliding drops into account.

In [7], the Lattice-Boltzmann method (LBM) was used to study drop deformation in electric fields. The most attractive feature of the LBM for multiphase flow is that no explicit treatment of the interface is needed. Briefly, the main idea of the LBM is to model the flow on a mesoscopic scale. A particle distribution function is introduced whose evolution is governed by the collisions and propagation of the particles moving on a lattice. In order to simulate multiphase flows, a particle interaction force is introduced between the two components, which mimics the effect of a repulsive force. However, the resulting interface is diffusive, i.e. it is a transitional region where the jumps in physical properties

Manuscript received on 28 May 2008, in final form 18 December 2008.

across the interface are smeared out. Unfortunately, in [7], the accuracy of this approach was not evaluated directly, but some discrepancies in the induced flow field compared to theory for a drop in an electric field were found, and these were attributed to the use of a diffuse interface.

A third method that has recently been used for simulating electrohydrodynamic flows is the coupled level-set and volume-of-fluid (CLSVOF) method [8]. In the level-set method [9, 10], the surface is described via an implicit function defined as the signed distance to the interface. This allows automatic handling of topological changes, along with simple calculation of normal vectors and curvature. A disadvantage with the method is that it does not inherently conserve mass. The VOF method uses a volume-fraction function to describe the interface. This approach ensures good mass conservation, but it is complicated to calculate the curvature accurately. In addition, the position of the interface is not known exactly, but is constructed using splines. The CLSVOF method combines the advantages of the two methods, and eliminates some of the disadvantages. The method was used in [11] to investigate electrohydrodynamic effects on film boiling in perfect dielectrics and in [12], the method was used on the leaky dielectric model and some accuracy tests were performed. In both papers, the continuous-surface-force (CSF) approach was used to handle surface-tension forces and electric forces. In this approach, a Heaviside function is used to smear the properties in a region around the interface. In [12], it was shown that by using a modified approach to the smearing of electrical properties, the accuracy was improved considerably.

The method used in the present work was proposed in [13, 14]. It also uses the level-set method to capture the interface, but instead of using a Heaviside function to treat the discontinuities, the ghost-fluid method (GFM) [15,16] is used. The ghost-fluid method modifies the numerical stencils near the interface to directly take the discontinuities into account. This gives improved accuracy in the computation of surface forces. The high accuracy also significantly reduces the errors in mass conservation.

In [14], the ability of the method to simulate drop oscillations, drop breakup, and drop-drop coalescence due to electric fields were presented. However, no test cases were performed that quantitatively measured the accuracy of the method. This work attempts to give a thorough evaluation of the method, comparing it to the test cases used in [12] and also to theoretical results for drop deformation. The discussion is limited to perfect dielectric fluids. It is possible to employ the method on the leaky-dielectric model as well, but that is more complex due to jumps in tangential stresses across the interface, and hence beyond the scope of this work.

2 GOVERNING EQUATIONS AND NUMERICAL METHODS

The numerical method used for the calculations is described in detail in [13, 14], and will only be briefly reviewed here. The full Navier-Stokes equations are solved in each phase, and the interface between the two phases is captured using the level-set method. The ghost-fluid method is used to treat discontinuities across the interface in a sharp manner. To account for electric forces, a Poisson equation is solved for the electric potential, which is then used to calculate the jump in the Maxwell stress tensor across the interface.

2.1 FLOW EQUATIONS

The flow is governed by the incompressible Navier-Stokes equations, with additional terms accounting for surface-tension forces and electric forces:

$$\rho\left(\frac{\partial \mathbf{u}}{\partial t}+(\mathbf{u}\cdot\nabla)\mathbf{u}\right)=-\nabla p+\nabla\cdot[\mu(\nabla\mathbf{u}+\nabla\mathbf{u}^{T})]+\mathbf{F}+\nabla\cdot\boldsymbol{M},\qquad \nabla\cdot\mathbf{u}=0. \tag{2.1}$$

Here, ρ is the density, $\mathbf{u}$ is the velocity vector, p is the pressure, μ is the viscosity, $\mathbf{F}$ is the surface-tension force and $\boldsymbol{M}$ is the Maxwell stress tensor.

The surface tension force, due to the presence of an interface, Γ, can be expressed by

$$\mathbf{F}(\mathbf{x},t)=\int_{\Gamma(t)}\mathbf{f}(s,t)\delta(\mathbf{x}-\mathbf{X}(s,t))\boldsymbol{d}s, \tag{2.2}$$

where s is the arc-length, $\mathbf{X}(s,t)$ is the parameterization of the interface, $\mathbf{x}$ is the spatial position and δ is the Dirac delta function. $\mathbf{f}$ is given by

$$\mathbf{f}=\sigma\kappa\mathbf{n}. \tag{2.3}$$

Here, σ denotes the surface-tension coefficient, κ is the curvature of the interface, and $\mathbf{n}$ is the unit normal vector.

In this work, all equations are solved in an axisymmetric geometry, so that the divergence operator and Laplacian operator become

$$\nabla\cdot\mathbf{f}=\frac{\partial f_x}{\partial x}+\frac{\partial f_y}{\partial y}+\frac{f_x}{x} \tag{2.4}$$

and

$$\nabla\cdot(\nabla\mathbf{f})=\frac{\partial^2\mathbf{f}}{\partial x^2}+\frac{\partial^2\mathbf{f}}{\partial y^2}+\frac{1}{x}\frac{\partial\mathbf{f}}{\partial x}, \tag{2.5}$$

respectively. Note that the subscripts indicate the vector component, and not the partial derivative of the vector. In addition to the above Laplace operator, one has to add $-f_x/x^2$ to the viscous term in the x-momentum equation.

2.2 ELECTRIC FORCES

We assume perfect dielectric materials with no free charges. With these assumptions, the electric potential, Ψ, can be calculated from the following Laplace equation:

$$\nabla\cdot(\varepsilon\varepsilon_0\nabla\Psi)=0, \tag{2.6}$$

where $\varepsilon_0=8.8542$ pF/m is the vacuum permittivity and ε is

the relative permittivity of the fluid. The electric field can then be calculated as

$$\mathbf{E} = -\nabla\Psi, \tag{2.7}$$

and the Maxwell stress tensor as

$$\boldsymbol{M} = \varepsilon\varepsilon_0\left(\mathbf{EE} - \frac{1}{2}(\mathbf{E}\cdot\mathbf{E})\boldsymbol{I}\right). \tag{2.8}$$

Here, $\boldsymbol{I}$ is the identity tensor. With the above assumptions, $\boldsymbol{M} = \boldsymbol{0}$ everywhere except at the interface.

2.3 INTERFACE CAPTURING

The interface is captured using the level-set method [9,10]. This method allows accurate computation of the evolution of an interface, along with automatic handling of topological changes. The ghost-fluid method [15, 16] is used to take discontinuities across the interface into account. This method handles the jumps in physical properties directly in the numerical stencils, without the need for any smearing of properties.

The interface is defined by the zero level set

$$\Gamma = \{\mathbf{x} \mid \phi(\mathbf{x}, t) = 0\}, \tag{2.9}$$

and is evolved by

$$\frac{\partial\phi}{\partial t} + \mathbf{u}_\Gamma\cdot\nabla\phi = 0. \tag{2.10}$$

Here, ϕ denotes the signed distance to the interface. $\mathbf{u}_\Gamma$ is the velocity on the interface. This velocity is not readily available, but in [17] it was shown that this velocity could be obtained by extrapolating the velocity orthogonally from the interface. This is achieved by solving

$$\frac{\partial\mathbf{u}}{\partial\tau} + S(\phi_0)\mathbf{n}\cdot\nabla\mathbf{u} = 0, \tag{2.11}$$

where τ is a pseudo-time and S is a sign function. Here,

$$S(\phi) = \frac{\phi}{\sqrt{\phi^2 + 2\Delta x^2}} \tag{2.12}$$

is used. Note that equation (2.11) is hyperbolic, so it is not necessary to solve it to steady state, since only the information a few grid points away from the interface is relevant to the evolution of the interface.

The standard level-set reinitialization procedure presented in [9] is used to keep the level-set function as a signed distance function throughout the computation. This is accomplished by solving

$$\begin{gathered}\frac{\partial\phi}{\partial\tau} + S(\phi_0)(|\nabla\phi| - 1) = 0 \\ \phi(\mathbf{x}, 0) = \phi_0(\mathbf{x}).\end{gathered} \tag{2.13}$$

Reinitialization is performed every second time step.

One of the advantages with the level-set method is the easy calculation of normal vectors and curvatures. The unit normal vector can be found as

$$\mathbf{n} = \frac{\nabla\phi}{|\nabla\phi|}, \tag{2.14}$$

and the curvature as

$$\kappa = -\nabla\cdot\mathbf{n}. \tag{2.15}$$

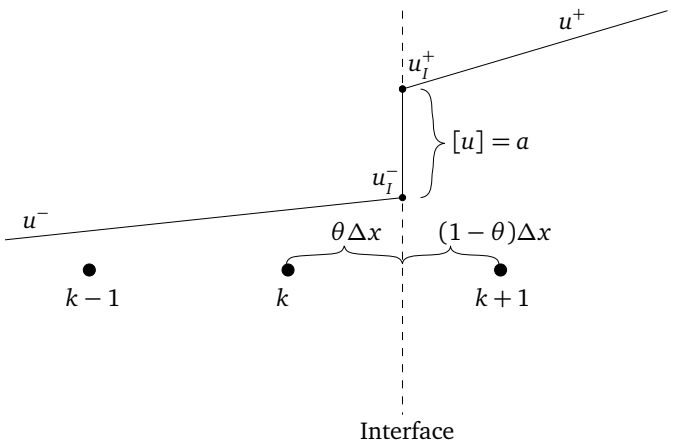

Figure 1. Illustration of the discretization of a discontinuous variable across an interface.

The ghost-fluid method will be illustrated here by considering the discretization of the following 1D Poisson equation:

$$\frac{du}{dx}\left(\beta\frac{du}{dx}\right) = f. \tag{2.16}$$

The ghost-fluid method requires jump conditions, which are relations between the physical quantities on each side of the interface. In the following, the interfacial jump is denoted by $[x] = x^+ - x^-$, where x^+ is the interfacial value on the side of the interface where ϕ is positive, and x^- is on the other side. For the purpose of this section, we assume that the interface conditions are given by

$$[u] = a \tag{2.17}$$

and

$$\left[\beta\frac{du}{dx}\right] = b. \tag{2.18}$$

Suppose that we have the condition given in Figure 1, where an interface is located between k and $k+1$. Instead of using the standard, second-order discretization

$$\frac{\beta_{k+1/2}\dfrac{u_{k+1} - u_k}{\Delta x} - \beta_{k-1/2}\dfrac{u_k - u_{k-1}}{\Delta x}}{\Delta x} = f_k \tag{2.19}$$

we would like to use the value at the interface,

$$\frac{\hat{\beta}\dfrac{u_I^- - u_k}{\theta\Delta x} - \beta_{k-1/2}\dfrac{u_k - u_{k-1}}{\Delta x}}{\Delta x} = f_k \tag{2.20}$$

where θ is the normalized distance to the interface,

$$\theta = \frac{x_I - x_k}{\Delta x} \tag{2.21}$$

An approximation of the interfacial value can be found by using the jump conditions. Discretizing equation (2.18) gives

$$\beta^+\frac{u_{k+1} - u_I^+}{(1-\theta)\Delta x} - \beta^-\frac{u_{k+1} - u_I^-}{\theta\Delta x} = b. \tag{2.22}$$

We can now find the approximated value at the interface by using equation (2.17):

$$u_I^- = \frac{1}{\theta\beta^+ + (1-\theta)\beta^-}[\theta\beta^+ u_{k+1} + (1-\theta)\beta^- u_k - \theta\beta^+ a - \theta(1-\theta)\Delta x b]. \quad (2.23)$$

Finally, this can be inserted into (2.20) to give the following symmetric discretization:

$$\frac{\hat{\beta}(u_{k+1}-u_k) - \beta^-(u_k - u_{k-1})}{\Delta x^2} = f_k + \frac{\hat{\beta}a}{\Delta x^2} + \frac{(1-\theta)\hat{\beta}b}{\beta^+ \Delta x} \quad (2.24)$$

where $\hat{\beta}$ denotes the extrapolated value of the coefficient,

$$\hat{\beta} = \frac{\beta^+\beta^-}{\theta\beta^+ + (1-\theta)\beta^-}. \quad (2.25)$$

This method can be applied in a dimension-by-dimension fashion, so an extension to two and three dimensions is trivial.

The jump conditions for viscous, incompressible flow is given in [16] and for dielectric fluids in [13]. The jump in pressure is

$$[p] = 2[\mu]\mathbf{n}\cdot\nabla\mathbf{u}\cdot\mathbf{n} + \mathbf{n}\cdot[\boldsymbol{M}]\cdot\mathbf{n} + \sigma\kappa\mathbf{n}\cdot\mathbf{n}. \quad (2.26)$$

The jumps in velocities are

$$[\mathbf{u}] = 0,$$
$$[\mu\nabla\mathbf{u}] = [\mu]\mathbf{n}\cdot\nabla(\mathbf{u}\cdot\mathbf{n})\mathbf{n}\mathbf{n} + [\mu]\mathbf{t}\cdot\nabla(\mathbf{u}\cdot\mathbf{n})\mathbf{n}\mathbf{t} - [\mu]\mathbf{t}\cdot\nabla(\mathbf{u}\cdot\mathbf{n})\mathbf{t}\mathbf{n} + [\mu]\mathbf{t}\cdot\nabla(\mathbf{u}\cdot\mathbf{t})\mathbf{t}\mathbf{t}. \quad (2.27)$$

For the electric potential, the jump conditions for perfect dielectrics are

$$[\Psi] = 0,$$
$$[\varepsilon\varepsilon_0\nabla\Psi\cdot\mathbf{n}] = 0. \quad (2.28)$$

2.4 NUMERICS

A second-order projection scheme is used to solve the Navier-Stokes equations. First, a temporary vector field, $\mathbf{a}$, is calculated:

$$\mathbf{a} = -(\mathbf{u}\cdot\nabla)\mathbf{u} + \nabla\cdot[\mu(\nabla\mathbf{u} + \nabla\mathbf{u}^T)]. \quad (2.29)$$

Then the pressure is found by solving

$$\nabla\cdot\left(\frac{\nabla p}{\rho}\right) = \nabla\cdot\mathbf{a}. \quad (2.30)$$

Finally, the velocity field is calculated with

$$\frac{\partial\mathbf{u}}{\partial t} = \mathbf{a} - \frac{\nabla p}{\rho}. \quad (2.31)$$

The evolution in time for the Navier-Stokes equations, the level-set equation and the velocity extrapolation is performed using a four-step, third-order, strong stability preserving (SSP) Runge-Kutta (RK) method (see e.g. [18]), while a four-step, second order SSP RK method is employed for the reinitialization of the level-set equation. The equations are spatially discretized on a staggered grid, with scalar values stored in cell centers and vector values stored at cell boundaries. The convective terms are discretized using the fifth order Weighted Essentially Non-Oscillatory (WENO) scheme [19], and viscous terms are discretized using standard second-order central differences.

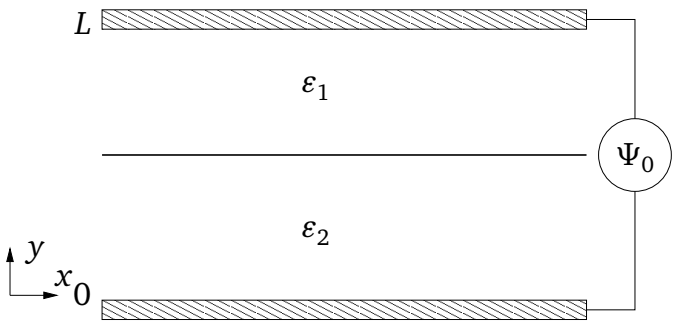

Figure 2. Configuration of the horizontal-interface test case.

3 METHOD EVALUATION

This section compares results from the CSF approach used in [12] and [11] with results from the sharp-interface method used here. The first test case is a horizontal interface in an electric field. This test case tests the ability of the numerical method to accurately predict the jumps across an interface. Then, results for the deformation of a dielectric drop subject to an electric field are presented.

3.1 A HORIZONTAL INTERFACE IN AN ELECTRIC FIELD

An interface is placed between two parallel plates, the upper medium has permittivity ε_1 and the lower medium has permittivity ε_2. The upper parallel plate is given a potential Ψ_0 while the lower plate is grounded. This configuration is illustrated in Figure 2. This test case is excellent for evaluating the handling of the discontinuity in electrical properties, and was considered in both [12] and [11]. In [11], an arithmetic mean is used to find the smoothed electric permittivities, while in [12], it was shown that using a harmonic mean gives significantly better results. In this section, these results are compared to the results obtained with the ghost-fluid method.

The equation for the electric potential is a Laplace equation with constant coefficients in each phase. This equation can be solved by noting that the potential is continuous across the interface (equation (2.28)). The solution is

$$\Psi_1 = 2\Psi_0\frac{1}{\varepsilon_1/\varepsilon_2 + 1}\frac{y-L}{L} + \Psi_0$$
$$\Psi_2 = 2\Psi_0\frac{1}{1+\varepsilon_2/\varepsilon_1}\frac{y}{L}. \quad (3.1)$$

The electric field in each phase can then be found by using equation (2.7):

$$E_1 = -\frac{2\Psi_0}{L}\frac{1}{\varepsilon_1/\varepsilon_2 + 1}$$
$$E_2 = -\frac{2\Psi_0}{L}\frac{1}{1+\varepsilon_2/\varepsilon_1}. \quad (3.2)$$

The pressure jump is given by equation (2.26), which for this case is

Table 1. Physical properties and analytical values for the horizontal-interface test case.

Quantity	Value
Plate distance, L	0.01
Permittivity 1, ε_1	70
Permittivity 2, ε_2	1
Potential difference, Ψ_0	100
Electric field 1, E_1	-2.8169×10^{2}
Electric field 2, E_2	-1.9718×10^{4}
Pressure jump, $[p]$	-1.6959×10^{-3}

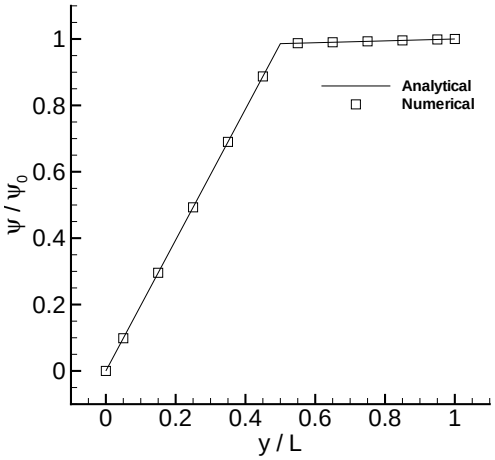

Figure 3. The horizontal-interface test case. The electric potential in the *y*-direction, scaled by the potential difference, for a calculation with 10 grid points.

$$[p] = \mathbf{n}\cdot[\boldsymbol{M}]\cdot\mathbf{n} = \frac{1}{2}\varepsilon_0(\varepsilon_1 E_1^2 - \varepsilon_2 E_2^2). \qquad (3.3)$$

We now analyze the accuracy of the ghost-fluid method for this test case. The chosen physical parameters along with the computed analytical solutions are given in Table 1, and are equivalent to those used in [12].

The ghost-fluid method uses an extrapolated value for the value at the interface in the discretization. Because the solution is linear in this particular case, this should give an exact solution for all grid sizes. Figure 3 shows the solution for the potential for a grid with 10 grid points, compared with the analytical solution. The 2-norm of the relative error is 5.29×10^{-16}, which means that the electric potential is accurately solved to machine precision, as expected. In [11] and [12], data is not provided for the accuracy of the CSF method when applied to the horizontal-interface test case. We found that for 10 grid points, the 2-norm of the relative error was 0.85% when using a harmonic mean to smear the permittivities, and 65.9% when using an arithmetic mean.

For the error of the electric field of phase 1, together with the error in the pressure jump, [12] report 4.8×10^{-3} % and 9.7×10^{-3} %, respectively, for a 40-point grid. We use the ghost-fluid method for calculating the gradient of the potential and for the discretization of the pressure equation, so again we expect an exact solution for all grid sizes for this particular test case. Figure 4 and Figure 5 show the computed solutions of the electric field and the pressure, respectively, together with the analytical solutions, for a grid with 10 points. The relative error for the value of the electric field was 2.21×10^{-15} and the error for the pressure jump was 7.64×10^{-15}. Clearly, the ghost-fluid method is significantly better than the CSF method for this test case.

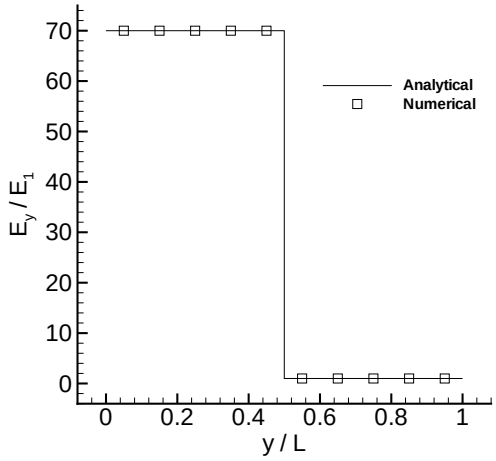

Figure 4. The horizontal-interface test case. The electric field in the *y*-direction, scaled by the exact solution for phase 1, for a calculation with 10 grid points.

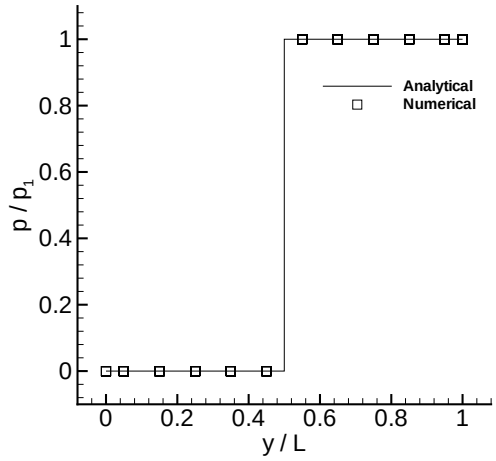

Figure 5. The horizontal-interface test case. The pressure in the *y*-direction, scaled by the exact solution for phase 1, for a calculation with 10 grid points.

3.2 A SPHERICAL DROP SUBJECT TO AN ELECTRIC FIELD

This test case serves to assess the accuracy of the ghost-fluid method for an axisymmetric problem. Finding the potential around a dielectric sphere in an electric field is a classical problem in electrodynamics (see e.g. [20]), with the following solution in spherical coordinates:

$$\Psi_{\text{an}}(r,\theta)=\begin{cases} -\dfrac{3}{\bar{\varepsilon}+2}E_0 r\cos\theta & \text{if } r\le R; \\ \left(\dfrac{\bar{\varepsilon}-1}{\bar{\varepsilon}+2}\dfrac{R^3}{r^3}-1\right)E_0 r\cos\theta & \text{if } r>R. \end{cases} \tag{3.4}$$

Here, $\bar{\varepsilon}$ is the permittivity ratio between the drop and the surrounding medium. The electric field is then

$$E_x(r,\theta)=\begin{cases} 0 & \text{if } r\le R; \\ -\dfrac{3}{2}\dfrac{\bar{\varepsilon}-1}{\bar{\varepsilon}+2}\dfrac{R^3}{r^3}E_0\sin 2\theta & \text{if } r>R. \end{cases}$$

$$E_y(r,\theta)=\begin{cases} \dfrac{3}{\bar{\varepsilon}+2}E_0 & \text{if } r\le R; \\ \left[\dfrac{\bar{\varepsilon}-1}{\bar{\varepsilon}+2}\dfrac{R^2}{r^3}\left(3\sin^2\theta-1\right)+1\right]E_0 & \text{if } r>R. \end{cases} \tag{3.5}$$

Note that this is the electric field in the x-direction and y-direction, but defined using r and θ for the purpose of a more compact presentation. These values can be compared to those found by the present algorithm by taking only one time step, so that there is no deformation of the sphere. The physical properties used for the test case is given in Table 2. A domain size of $3R\times 6R$ was used. The error in the potential, together with the convergence behavior, is given in Table 3. The order of convergence is defined as

$$\text{O}=\frac{\ln(E_2/E_1)}{\ln(N_2/N_1)}, \tag{3.6}$$

Where E_i is the error on a grid with N_i grid points. The error is low even for small grid sizes, and the convergence is that expected of the ghost-fluid method.

Figure 6 shows a comparison of the potential contour lines for the analytical and numerical result. Figure 7, which shows stream-traces of the electric field, further demonstrates the accuracy of the ghost-fluid method.

Table 2. Physical properties and analytical values for the spherical-drop test case.

Quantity	Value
Drop radius, R	1×10^{-3}
Surface tension, σ	32×10^{-4}
Permittivity 1, ε_1	10
Permittivity 2, ε_2	1
Initial electric field, E_0	3.4543×10^{5}

Table 3. The 2-norm of the error in the potential for the spherical-drop test case, along with the order of convergence.

R/h	$\lvert\Psi-\Psi_{\text{an}}\rvert$ ($\times10^{-6}$ V)	Order
5	23.1	-
10	12.3	0.91
20	7.59	0.70
40	3.69	1.04

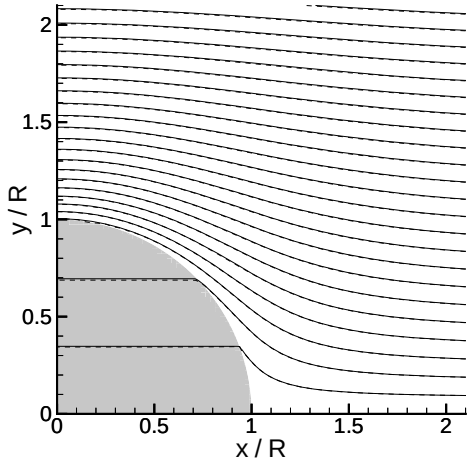

Figure 6. The spherical-drop test case. Comparison of analytical (solid) and numerical (dashed) potential around a dielectric drop for $R/h=40$.

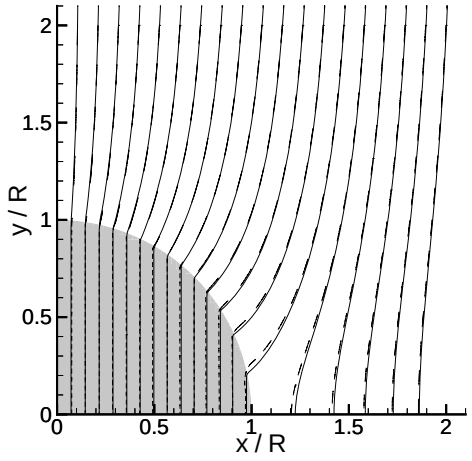

Figure 7. The spherical-drop test case. Comparison of analytical (solid) and numerical (dashed) electric field around a dielectric drop for $R/h=40$.

In [12], they compared the pressure jump across the interface along the x-axis, where the jump in pressure is the highest, to the theoretical result. The pressure jump is given by equation (2.26), which for this particular problem becomes

$$[p]=\frac{2\sigma}{R}-\frac{9}{2}\frac{\bar{\varepsilon}-1}{(\bar{\varepsilon}+2)^2}\varepsilon_0 E_0^2 \tag{3.7}$$

The error for the maximum pressure jump when using the ghost-fluid method is given in Table 4. For $R/h=10$, the

Table 4. The relative error for the maximum pressure jump across the interface of a spherical drop.

R/h	Relative error, $[p]$ ($\times10^{-3}$ Pa)	Order
5	8.74	-
10	3.38	1.37
20	1.63	1.05
40	0.482	1.76

error is nearly equal to that reported in [12] for $R/h = 160$. This shows the superiority of the sharp-interface approach compared to the smeared-interface approach. The convergence behavior is similar for the two methods.

3.3 DEFORMATION OF A SPHERICAL DROP SUBJECT TO AN ELECTRIC FIELD

If an electric field is applied to an initially spherical drop in a matrix fluid of different permittivity, the drop will deform. As explained in [2], a perfect dielectric drop will always stretch in the direction of the electric field. The amount of stretching depends on the permittivity ratio, $\bar{\varepsilon}$, and the ratio between electric forces and capillary forces, expressed by the dielectric Bond number,

$$\mathrm{Bo}_\mathrm{e} = \frac{\varepsilon_2 \varepsilon_0 D}{\sigma} E_0^2. \tag{3.8}$$

An expression for the steady-state deformation was found in [21], by an energetic approach. Good agreement with finite-element computations was reported. The expression can be written as

$$\begin{aligned}
\mathrm{Bo}_\mathrm{e} &= \frac{4a^2 e - 2a^{7/2}\sin^{-1} e + 6a^{1/2}e^{-2}\sin^{-1} e - 6a^2 e^{-1}}{\left(\dfrac{\bar{\varepsilon}-1}{1+n(\bar{\varepsilon}-1)}\right)^2 \left(\dfrac{-2ne}{1-e^2} - 3ne^{-1} + e^{-1}\right)} \\
n &= \frac{1-e^{-2}}{e^3}\left(\ln\sqrt{\frac{1+e}{1-e}} - e\right) \\
e^2 &= 1 - b^2/a^2 \\
b^2 &= R_0^3/a
\end{aligned} \tag{3.9}$$

For permittivity ratios above approximately 20, the elongation is no longer single-valued, and hysteresis may occur. The parameter range that allows hysteresis is very narrow, $20 \le \bar{\varepsilon} \le 25$. For other values, the drop shape is unstable, and the drop will begin to emit small drops from its tips to lower its radius and thereby reattain a stable value. A series of numerical calculations were performed to compare the numerical method to the above theoretical result. To avoid having to run the simulations to steady state, the simulations were run for one oscillation period with viscosities equal to zero, and the average between the maximum and the minimum value was used as the steady state value. This will not be entirely correct due to numerical diffusion, but is considered sufficient for the present purpose. The computational domain was $3R_0 \times 9R_0$, and a grid size of 160×481 was used. For this grid size, the relative error in using the values for an inviscid computation compared to running to steady state was found to be 1.3×10^{-3} for $\mathrm{Bo}_\mathrm{e} = 0.05$ when using the ghost-fluid method.

A comparison between the theoretical values and the computational values for the ratio of the semi-major and the semi-minor axes are given in Figure 8. The CSF results are computed using the approach from [11], with permittivities approximated using harmonic mean. The results for the ghost-fluid method are significantly closer to the theoretical predictions than the results for the CSF approach.

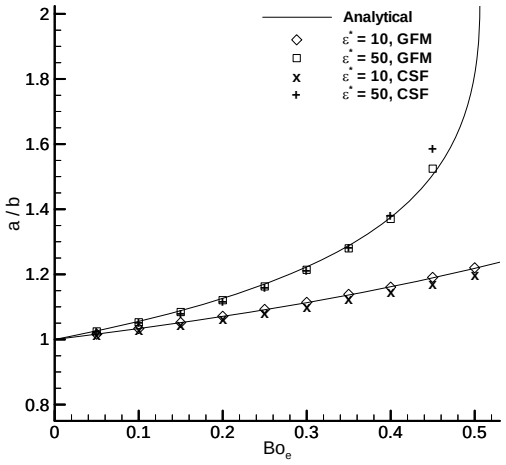

Figure 8. Deformation of spherical-drop test case. Comparison of the deformation between the theoretical values given by equation (3.9) and the numerical results for varying dielectric Bond number and permittivity ratios.

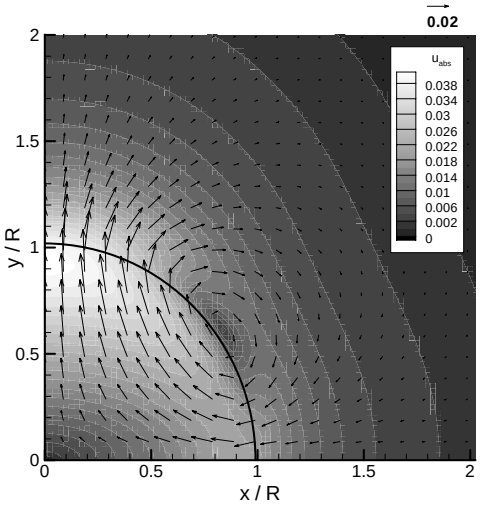

Figure 9. The prolate shape and induced flow field for $\mathrm{Bo}_\mathrm{e} = 0.05$ and $\bar{\varepsilon} = 10$ when velocities are at a maximum. The contours show velocity magnitude. $\rho_1 = \rho_2 = 100\,\mathrm{kg/m^3}$, $\sigma = 1$ N/m, $\mu_1 = \mu_2 = 0.01\,\mathrm{Pa\,s}$.

An example of the induced flow field is given in Figure 9. This is when the flow field reaches a maximum, just before the surface-tension forces begin reversing the flow. Note that the velocity is highest towards the pole of the drop. For high field strengths, this can lead to conical ends, as shown in [22]. The flow tends to zero as the droplet reaches its equilibrium shape.

Since the electric field is abruptly applied at $t = 0$, inertia will cause the drop to overshoot the asymptotic value for the deformation, and then oscillate about this value until the viscous effects have damped out the motion. This overshoot may cause the drop to become unstable at values lower than those predicted by equation (3.9). For the values used here, the theoretical expression predicts breakup at $\mathrm{Bo}_\mathrm{e} \approx 0.522$. However, at $\mathrm{Bo}_\mathrm{e} \approx 0.5$, the numerical calculations no longer reach a steady-state value. Predicting when breakup occurs

will then no longer be a function of just Bo_e and $\bar{\varepsilon}$, but will also depend on the viscosities and densities of the two media. Investigating such a criterion is beyond the scope of this work.

4 CONCLUSION

This work presented an evaluation of a sharp-interface approach to simulating two-phase, electrohydrodynamic flows. The sharp-interface method was shown to give significant improvements in accuracy compared to smeared-interface approaches.

The generality of the method allows it to be used in a wide range of problems involving two-phase flows and electric fields. The inherent handling of topological changes makes the method attractive for studying problems involving breakup or coalescence, for instance film boiling and emulsion stability.

Only perfect dielectric fluids were considered in this work. A natural extension is to apply the method to the leaky dielectric model. This will be presented in a future work.

ACKNOWLEDGMENT

This work is funded by the project "Electrocoalescence -- Criteria for an efficient process in real crude oil systems"; coordinated by SINTEF Energy Research. The project is supported by The Research Council of Norway, under the contract no: 169466/S30, and by the following industrial partners: Aibel AS, Aker Solutions AS, BP Exploration Operating Company Ltd, Saudi Aramco, Shell Technology Norway AS, StatoilHydro ASA and Petrobras.

The authors thank Joris Verschaeve for interesting discussions regarding the Lattice-Boltzmann method. Further, the constructive comments of the referees have improved the article.

REFERENCES

[1] J. Sherwood, "Breakup of fluid droplets in electric and magnetic fields", J. Fluid Mech, Vol. 188, pp. 133–146, 1988.

[2] J. Baygents, N. Rivette, and H. Stone, "Electrohydrodynamic deformation and interaction of drop pairs", J. Fluid Mech., Vol. 368, pp. 359–375, 1998.

[3] T. Tsudaka, Y. Yamamoto, T. Katayama and M. Hozawa, "Theoretical and experimental studies of circulations inside and outside a deformed drop moving in a quiescent liquid", J. Chem. Engng. Japan, Vol. 27, pp. 662-666, 1994.

[4] J. Q. Feng, and T. C. Scott, "A computational analysis of electrohydrodynamics of a leaky dielectric drop in an electric field", J. Fluid Mech., Vol. 311, pp. 289-326, 1996.

[5] S.O. Unverdi, and G. Tryggvason, "A front-tracking method for viscous, incompressible, multi-fluid flows", J. Comp. Phys., Vol. 100, pp. 25–37, 1992.

[6] A. Fernandez, G. Tryggvason, J. Che, and S. Ceccio, "The effects of electrostatic forces on the distribution of drops in a channel flow: two-dimensional oblate drops", Phys. Fluids, vol. 17, No. 093302. 2005.

[7] J. Zhang and D.Y. Kwok, "A 2D lattice Boltzmann study on electrohydrodynamic drop deformation with the leaky dielectric theory", J. Comput. Phys., Vol. 206, pp. 150–161, 2005.

[8] M. Sussman and E.G. Puckett, "A coupled level set and volume-of-fluid method for computing 3D and axisymmetric incompressible two/phase flows", J. Comput. Phys., Vol. 162 , pp. 301–337, 2000.

[9] M. Sussman, P. Smereka, and S. Osher, "A level set approach for computing solutions to incompressible two-phase flow", J. Comput. Phys., Vol. 114, pp. 146–159, 1994.

[10] S. Osher and R. Fedkiw, *Level Set Methods and Dynamic Implicit Surfaces*. Springer, 2003.

[11] S. Welch and G. Biswas, "Direct simulation of film boiling including electrohydrodynamic forces", Phys. Fluids, Vol. 19, No. 012106, 2007.

[12] G. Tomar, D. Gerlach, G. Biswas, N. Alleborn, A. Sharma, D. Durst, S. Welch, and A. Delgado, "Two-phase electrohydrodynamic simulations using a volume-of-fluid approach", J. Comput. Phys., Vol. 227, pp. 1267–1285, 2007.

[13] E. B. Hansen, "*Numerical Simulation of Droplet Dynamics in the Presence of an Electric Field*", Ph.D. dissertation, Norwegian University of Science and Technology (NTNU), 2005.

[14] E. Bjørklund, "The level-set method applied to droplet dynamics in the presence of an electric field", Comput. Fluids, Vol. 38, pp. 358-369, 2009.

[15] R. Fedkiw, "A non-oscillatory Eulerian approach to interfaces in multimaterial flows", J. Comput. Phys., Vol. 152, pp. 457–492, 1999.

[16] M. Kang, R. Fedkiw, and X. Liu, "A boundary condition capturing method for multiphase incompressible flow", J. Sci. Comput., Vol. 15, pp. 323–360, 2000.

[17] H. K. Zhao, T. Chan, B. Merriman, and S. Osher, "A variational level set approach to multi-phase motion", J. Comput. Phys., Vol. 127, pp. 179-195, 1996.

[18] J. F. B. M. Kraaijevanger, "Contractivity of Runge-Kutta methods", BIT (Nordisk tidskrift for informationsbehandling) Num. Math., Vol. 31, pp. 482-528, 1991.

[19] G. Jiang and D. Peng, "Weighted ENO schemes for Hamilton-Jacobi equations", Society for Industrial and Applied Mathematics (SIAM) J. Sci. Comp., Vol. 21, pp. 2126–2143, 2000.

[20] D. Griffiths, *Introduction to electrodynamics*. Prentice-Hall, Inc, 1999.

[21] A. Ramos and A. Castellanos, "Equilibrium shapes and bifurcation of captive dielectric drops subjected to electric fields", J. Electrostatics, Vol. 33, pp. 61-86, 1994.

[22] G. Taylor, "Disintegration of Water Drops in an Electric Field", Proc. R. Soc. London Ser. A, Vol. 280, pp. 383-397, 1964.

Knut Erik Teigen was born in Norway in 1983. He received the M.S. degree in mechanical engineering from the Norwegian University of Science and Technology (NTNU) in 2007. Presently, he is a Ph.D. candidate at the Department of Energy and Process Engineering at NTNU. His research interests are computational fluid dynamics, in particular the numerical simulation of two-phase flows.

Svend Tollak Munkejord was born in Norway in 1974. He received the M.S. degree in mechanical engineering from NTNU in 1997, and the Ph.D. degree from the same university in 2006. Presently, he is a research scientist at SINTEF Energy Research. His research interests include the mathematical modeling and numerical analysis of two-phase flows.